 Related Commentary, page 763

A missense mutation in the Kv1.1 voltage-gated potassium channel–encoding gene *KCNA1* is linked to human autosomal dominant hypomagnesemia

Bob Glaudemans,[1] Jenny van der Wijst,[1] Rosana H. Scola,[2] Paulo J. Lorenzoni,[2] Angelien Heister,[3] AnneMiete W. van der Kemp,[1] Nine V. Knoers,[3] Joost G. Hoenderop,[1] and René J. Bindels[1]

[1]Department of Physiology, Radboud University Nijmegen Medical Centre, Nijmegen, The Netherlands. [2]Neuromuscular Disorders Division, Clinical Hospital, Parana Federal University, Curitiba, Parana, Brazil. [3]Department of Human Genetics, Radboud University Nijmegen Medical Centre, Nijmegen, The Netherlands.

Primary hypomagnesemia is a heterogeneous group of disorders characterized by renal or intestinal magnesium (Mg^{2+}) wasting, resulting in tetany, cardiac arrhythmias, and seizures. The kidney plays an essential role in maintaining blood Mg^{2+} levels, with a prominent function for the Mg^{2+}-transporting channel transient receptor potential cation channel, subfamily M, member 6 (TRPM6) in the distal convoluted tubule (DCT). In the DCT, Mg^{2+} reabsorption is an active transport process primarily driven by the negative potential across the luminal membrane. Here, we studied a family with isolated autosomal dominant hypomagnesemia and used a positional cloning approach to identify an N255D mutation in *KCNA1*, a gene encoding the voltage-gated potassium (K^+) channel Kv1.1. Kv1.1 was found to be expressed in the kidney, where it colocalized with TRPM6 along the luminal membrane of the DCT. Upon overexpression in a human kidney cell line, patch clamp analysis revealed that the *KCNA1* N255D mutation resulted in a nonfunctional channel, with a dominant negative effect on wild-type Kv1.1 channel function. These data suggest that Kv1.1 is a renal K^+ channel that establishes a favorable luminal membrane potential in DCT cells to control TRPM6-mediated Mg^{2+} reabsorption.

Introduction

Occurrence of hypomagnesemia (serum Mg^{2+} levels below 0.70 mmol/l) in the general population has been estimated to be around 2%, while hospitalized patients are more prone to develop hypomagnesemia (12%) (1). Recent studies of intensive care patients have even estimated frequencies as high as 60% (2). The blood Mg^{2+} concentration depends on the renal Mg^{2+} excretion in response to altered uptake by the intestine. Hence, the kidney is essential for the maintenance of the Mg^{2+} balance (3). The majority of filtered Mg^{2+} is reabsorbed along the proximal tubule and the thick ascending limb of Henle's loop via a passive paracellular pathway (4). However, fine-tuning of Mg^{2+} excretion occurs in the distal convoluted tubule (DCT) in an active transcellular fashion initiated by the Mg^{2+}-permeable transient receptor potential cation channel, subfamily M, member 6 (TRPM6) (5, 6). Since the extra- and intracellular Mg^{2+} concentrations are both in the millimolar range, it has been hypothesized that the membrane potential across the luminal membrane acts as the primary driving force for Mg^{2+} entry via TRPM6 (6, 7). Previously, genetic studies in families with hereditary renal Mg^{2+} wasting syndromes revealed several new genes involved in Mg^{2+} homeostasis, including tight junction proteins claudin 16 and 19 (8, 9), the thiazide-sensitive sodium chloride cotransporter (NCC) (10), the γ-subunit of the Na^+/K^+-ATPase (FXYD2) (11), TRPM6 (12, 13), and the recently discovered magnesiotropic hormone EGF (14). Despite these discoveries, our knowledge of renal Mg^{2+} handling remains far from complete.

In this study, we screened a Brazilian family with isolated autosomal dominant hypomagnesemia and identified a missense mutation in *KCNA1*, resulting in nonfunctionality of the encoded voltage-gated potassium channel Kv1.1.

Results

A heterozygous KCNA1 A763G mutation is causative for hypomagnesemia. Here, we identified a large Brazilian family (46 family members, of which 21 are affected) with autosomal dominant hypomagnesemia (Figure 1A). Affected individuals showed low serum Mg^{2+} levels (<0.40 mmol/l; normal range, 0.70–0.95 mmol/l), while their urinary Mg^{2+} excretion was normal, suggesting impaired tubular Mg^{2+} reabsorption. The phenotype of the proband (IV-3, Figure 1A) starting from infancy consists of recurrent muscle cramps, tetanic episodes, tremor, and muscle weakness, especially in distal limbs. An SNP-based linkage analysis identified a 14.3-cM locus on the short arm of chromosome 12 (Figure 1B), which was subsequently narrowed down by fine mapping with microsatellite markers to an 11.6-cM region containing 31 genes between the markers D12S1626 and D12S1623 (maximum multipoint lod score, 3.0) (Figure 1B and Supplemental Figure 1; supplemental material available online with this article; doi:10.1172/JCI36948DS1). Other genes previously associated with hypomagnesemia are located outside this critical region and therefore were excluded

Authorship note: Bob Glaudemans and Jenny van der Wijst contributed equally to this work.

Conflict of interest: The authors have declared that no conflict of interest exists.

Nonstandard abbreviations used: AQP2, aquaporin-2; CNT, connecting tubule; DCT, distal convoluted tubule; DTX-K, dendrotoxin K; EA1, episodic ataxia type 1; Kv1.1, voltage-gated potassium channel subtype 1.1; TRPM6, transient receptor potential cation channel, subfamily M, member 6.

Citation for this article: *J. Clin. Invest.* **119**:936–942 (2009). doi:10.1172/JCI36948.

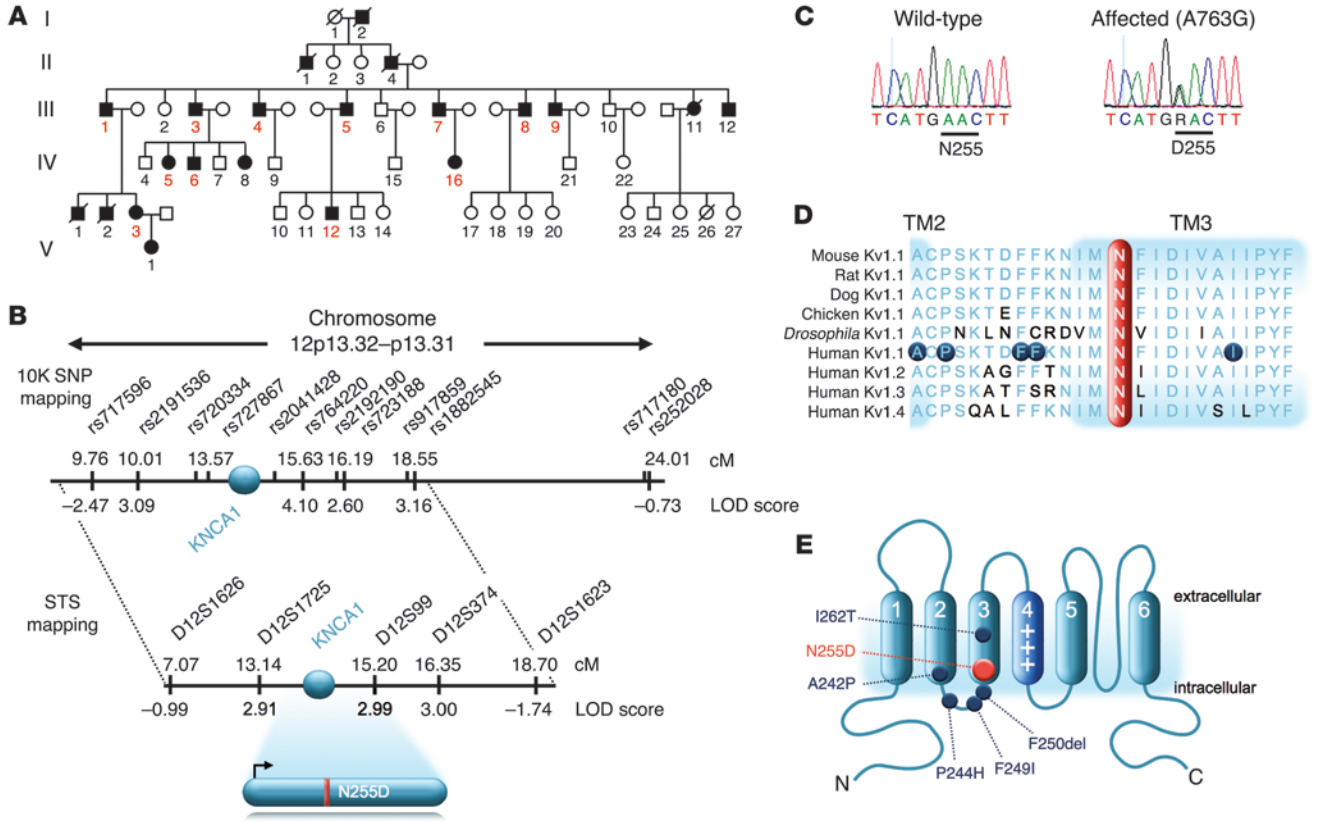

Figure 1

Heterozygous *KCNA1* A763G mutation causes isolated hypomagnesemia. (**A**) Pedigree with 5 generations (I–V) of a Brazilian family with autosomal dominant hypomagnesemia. Affected family members are indicated in black; males and females are indicated by squares and circles, respectively. A diagonal line indicates that the individual is deceased. Numbers in red indicate individuals included in the Sequence Tagged Site (STS) mapping. (**B**) 10K SNP array–based haplotyping analysis was performed that showed linkage to a 14.3-cM region between SNP rs717596 and rs252028 on the short arm of chromosome 12. This region was confirmed and narrowed down with STS markers to a 11.6-cM region between markers D12S1626 and D12S1623 containing 31 genes, including *KCNA1*. (**C**) *KCNA1* encodes the voltage-gated potassium channel Kv1.1. Mutation analysis of *KCNA1* revealed a heterozygous A763G missense mutation in affected individual III-1 that results in a N255D amino acid substitution (underlined). (**D**) Multiple alignment analysis shows conservation of the N255 amino acid (red bar) among species and Kv1 family members. Mutated amino acids in other families with the Kv1.1 genotype are indicated by dark blue dots (17, 19, 21, 22). Blue and black letters represent conserved and nonconserved amino acids, respectively. (**E**) Schematic representation of the Kv1.1 channel, which consists of a voltage sensor in transmembrane segment S4 and a pore-forming region (S5 and S6). Localization of the newly identified N255D mutation is denoted by the red dot, while other nearby mutations are indicated by dark blue dots.

as candidate genes in our family. From the identified locus, we sequenced *KCNA1* and identified a heterozygous mutation, A763G (Figure 1C), in the affected individual III-1 (Figure 1A) that cosegregates with the disorder and was absent in 100 control chromosomes (data not shown). The identified mutation in *KCNA1*, which encodes the Shaker-related voltage-gated K^+ channel Kv1.1, causes substitution of the highly conserved asparagine at position 255 for an aspartic acid (N255D) (Figure 1D). The predicted amino acid topology of Kv channels shows 6 transmembrane-spanning α-helical segments (i.e., S1–S6), with the S4 segment acting as the voltage sensor and a hydrophobic pore region between S5 and S6 (Figure 1E) (15). The newly identified N255D mutation is positioned in the third transmembrane segment (S3) close to the voltage sensor (Figure 1E).

Localization of Kv1.1 in the DCT of the kidney. So far, all proteins implicated in familial hypomagnesemia have been shown to be expressed in kidney, underlining the pivotal role of this organ in body Mg^{2+} homeostasis. To study the (sub)cellular localization of Kv1.1 in kidney, we used a rabbit polyclonal antibody raised against the Kv1.1 channel. Immunopositive staining was observed along the luminal membrane of distinct tubules present in the superficial cortex of the mouse kidney (Figure 2). Using serial kidney sections, we demonstrated that Kv1.1 colocalizes with the epithelial Mg^{2+} channel TRPM6 in DCT (Figure 2A). To confirm this localization, we costained kidney sections for Kv1.1 and calbindin D_{28K} and found a partial overlap in Kv1.1 and calbindin D_{28K} expression (Figure 2B). This pattern can be explained by earlier observations that calbindin D_{28K} is expressed not only in the DCT but also in connecting tubule (CNT) (16). Therefore, these data confirm that Kv1.1 is localized primarily in the DCT. Indeed, costaining between Kv1.1 and aquaporin-2 (AQP2), a marker for CNT and the collecting duct, was not observed (Figure 2C). These findings support the restricted localization of Kv1.1 in the Mg^{2+}-transporting DCT segment of the kidney.

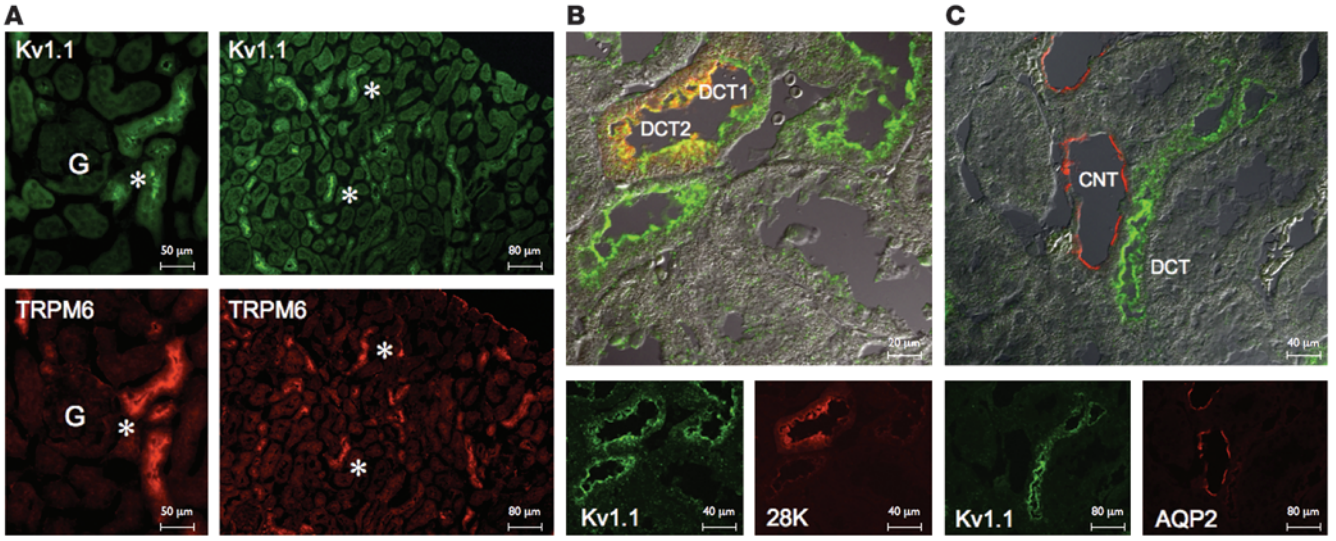

Figure 2
Immunohistochemical analysis of Kv1.1 in kidney. (**A**) Staining for Kv1.1 (green) and TRPM6 (red) of mouse serial kidney sections (right panels: overview of a cortical region; left panels: magnified images of immunopositive tubules). The asterisks indicate the same distal tubules on serial sections intensively stained for Kv1.1 and TRPM6. (**B**) Mouse kidney sections were costained for Kv1.1 (green) and calbindin D_{28K} (red) (lower panels: immunopositive tubules; upper panel: merged differential interference contrast [DIC] image). (**C**) Costaining of Kv1.1 (green) and AQP2 (red) in mouse kidney sections (lower panels: immunopositive tubules; upper panel: merged DIC image). G, glomerulus; 28K, calbindin D_{28K}. Scale bars: 50 μm (**A**, left panels), 80 μm (**A**, right panels; **C**, bottom panels), 20 μm (**B**, top panel), 40 μm (**B**, bottom panels; **C**, top panel).

Kv1.1 N255D results in nonfunctional channels with dominant negative effect on wild-type channel function. To determine the effect of the Kv1.1 N255D mutation on channel activity, HEK293 cells were mock transfected or were transiently transfected with wild-type Kv1.1 and/or Kv1.1 N255D. Using the whole-cell patch clamp technique, we measured outward K^+ currents by dialyzing the cells with a pipette solution containing 140 mM K^+. Cells expressing wild-type Kv1.1 channels produced typical delayed rectifying currents, while Kv1.1 N255D–expressing HEK293 cells showed small currents similar to those of mock plasmid–expressing cells (Figure 3, A and B). Considering the autosomal dominant inheritance in our family, we investigated a potential dominant negative effect by cotransfection of equal amounts of plasmid DNA encoding wild-type Kv1.1, Kv1.1 N255D, or mock plasmid in HEK293 cells. The K^+ current amplitude in HEK293 cells coexpressing wild-type Kv1.1 and Kv1.1 N255D was significantly reduced compared with that in cells expressing wild-type Kv1.1 alone or coexpressing wild-type Kv1.1 and mock plasmid ($P < 0.05$) (Figure 3C). Next, the influence of Kv1.1 N255D expression on the amount of Kv1.1 channels at the plasma membrane was examined by cell surface biotinylation experiments. As shown in Figure 3D, coexpression of wild-type Kv1.1 and Kv1.1 N255D in HEK293 cells did not affect the plasma membrane localization of Kv1.1 channels. Of note, Kv1.1 was equally expressed in all conditions as analyzed in the total cell lysates (Figure 3D, bottom panel). As Kv1.1 channels are composed of 4 subunits, this result suggests that similar amounts of both homotetrameric channels of wild-type Kv1.1 or Kv1.1 N255D, and heterotetrameric channels composed of wild-type Kv1.1 with Kv1.1 N255D are located at the plasma membrane.

Kv1.1 regulates TRPM6 Mg^{2+} influx by setting the membrane potential. Since Kv1.1 and TRPM6 are present in the same nephron segment, we investigated by which mechanism Kv1.1 controls Mg^{2+} influx through TRPM6. We studied the potential direct effect of Kv1.1 on TRPM6 activity by patch clamp analysis. To this end, TRPM6 (1.0 μg) was cotransfected with mock plasmid (0.1 μg), wild-type Kv1.1 (0.1 μg), or Kv1.1 N255D (0.1 μg) in HEK293 cells. The TRPM6-mediated Na^+ currents were virtually identical in the 3 experimental conditions (Figure 3E). Subsequently, the current clamp mode of the patch clamp technique was used to measure the membrane potential of HEK293 cells expressing wild-type Kv1.1 or Kv1.1 N255D. A significant hyperpolarization ($P < 0.05$) was observed in wild-type Kv1.1-expressing HEK293 cells (–39 ± 3 mV, $n = 9$) compared with mock plasmid– or Kv1.1 N255D–expressing cells (–3 ± 1 mV, $n = 7$, and –8 ± 2 mV, $n = 7$, respectively). Dendrotoxin K (DTX-K, 10 nM), a specific Kv1.1 channel blocker, significantly depolarized the membrane potential in wild-type Kv1.1-expressing cells (from –39 ± 3 mV to –14 ± 2 mV, $n = 8$, $P < 0.05$) (Figure 3F). The membrane potential of mock plasmid– or Kv1.1 N255D–expressing cells was not affected by DTX-K application (Figure 3F). Furthermore, cotransfection of wild-type Kv1.1 and Kv1.1 N255D resulted in an intermediate hyperpolarization compared with the cells expressing only wild-type Kv1.1 (–23 ± 1 mV vs. –39 ± 3 mV, respectively, $n = 15$, $P < 0.05$). These results suggest that compared with the normal Kv1.1 channel, the Kv1.1 N255D channel diminishes negative membrane potential.

Discussion

In this study, we identified a large Brazilian family with autosomal dominant hypomagnesemia. Affected individuals showed low serum Mg^{2+} levels, while serum K^+ and Ca^{2+} levels and urinary Ca^{2+} excretion were not affected, which is distinct from previously described forms of inherited hypomagnesemia. For example, members of families bearing a mutation in claudin 16 and claudin 19 (familial hypomagnesemia with hypercalciuria and

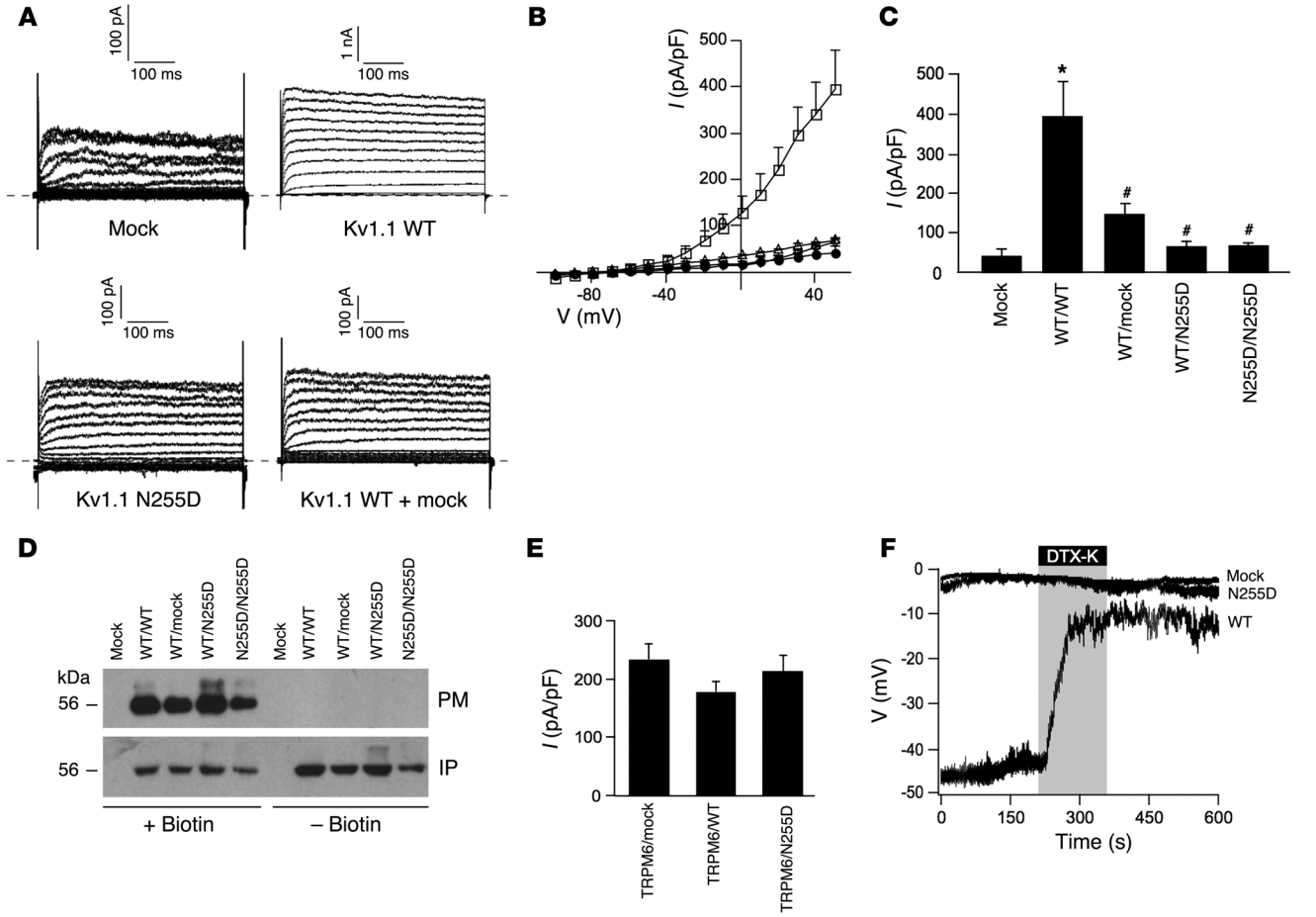

Figure 3

Electrophysiological analysis of HEK293 cells transfected with mock plasmid, wild-type Kv1.1 (Kv1.1 WT), or Kv1.1 N255D. (**A**) Representative original traces of outward K^+ currents of cells transfected with mock plasmid, Kv1.1 WT, Kv1.1 N255D, or Kv1.1 WT and mock plasmid elicited by voltage steps from –100 to +50 mV in 10-mV increments, applied from a holding potential of –80 mV, every 10 seconds. (**B**) The I-V relationships of cells transfected with mock plasmid (circles, $n = 5$), Kv1.1 WT (squares, $n = 11$), Kv1.1 N255D (triangles, $n = 10$), and Kv1.1 WT and mock plasmid (diamonds, $n = 9$). (**C**) Histogram presenting averaged current densities at +50 mV of cells transfected with mock plasmid ($n = 5$), Kv1.1 WT ($n = 11$), Kv1.1 WT and mock plasmid ($n = 9$), Kv1.1 WT and Kv1.1 N255D ($n = 9$), and Kv1.1 N255D ($n = 10$). $^*P < 0.05$, compared with mock; $^{\#}P < 0.05$, compared with Kv1.1 WT. (**D**) Cell surface biotinylation of HEK293 cells transfected with mock plasmid, Kv1.1 WT, Kv1.1 WT and mock plasmid, Kv1.1 WT and Kv1.1 N255D, and Kv1.1 N255D. Kv1.1 expression was analyzed by immunoblotting for plasma membrane fraction (PM) and input from the total cell lysates (IP). Representative immunoblot of 4 independent experiments is shown. (**E**) Histogram presenting averaged current densities at +80 mV after 200 seconds of cells cotransfected with TRPM6 and mock plasmid ($n = 26$), TRPM6 and Kv1.1 WT ($n = 26$), and TRPM6 and Kv1.1 N255D ($n = 25$). (**F**) Membrane potential of cells transfected with mock plasmid, Kv1.1 WT, and Kv1.1 N255D upon acute application of DTX-K (10 nM), measured in current clamp mode of whole-cell patch clamp configuration. Representative recordings of 8 independent experiments are shown. The error bars denote SEM.

nephrocalcinosis; OMIM 248250 and 248190) are hypercalciuric, while mutations in *FXYD2* (isolated dominant hypomagnesemia [IDH]; OMIM 154020) and *TRPM6* (hypomagnesemia with secondary hypocalcemia; OMIM 602014) result in hypocalciuria and hypocalcemia, respectively. Furthermore, patients with Gitelman syndrome (OMIM 263800), caused by mutations in NCC, suffer from hypomagnesemia, hypocalciuria, and hypokalemia. The phenotype in the proband starting from infancy consists of recurrent muscle cramps, tetanic episodes, tremor, and muscle weakness, especially in distal limbs. Serum electrolyte levels were measured during severe attacks of cramps and tetany in 2 affected family members (proband V-3; V-2), with serum Mg^{2+} levels of 0.37 and 0.25 mmol/l, respectively, while serum Ca^{2+} and K^+ concentrations were normal. As a result, all affected family members received a daily dose of magnesium chloride. Importantly, the proband was hospitalized during the course of this study because of a sudden episode of facial myokymia, tremor, severe muscle spasms, muscular pain, cramps, muscular weakness, and tetanic contraction episodes, all of which improved shortly after intravenous magnesium treatment. This observation further confirmed that the observed symptoms are a consequence of the low serum Mg^{2+} levels.

By use of a positional cloning approach, we revealed a heterozygous mutation in *KCNA1*, encoding the voltage-gate potassium channel Kv1.1, by which the asparagine at amino acid position 255 was converted into an aspartic acid (N255D). Remarkably, the Kv1.1 N255D genotype causes hypomagnesemia, whereas

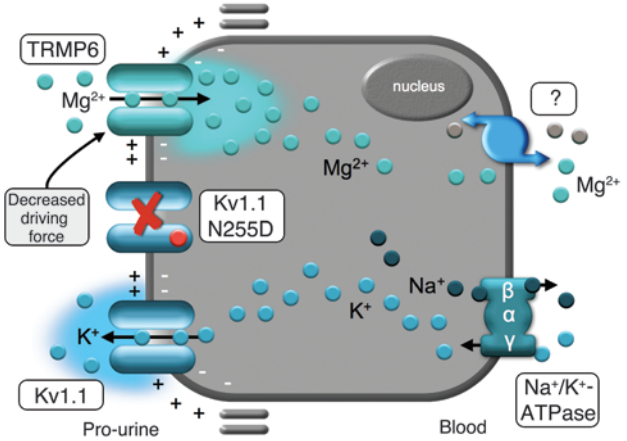

Figure 4
Schematic model of the Mg^{2+}-reabsorbing DCT cell in the kidney. Mg^{2+} uptake from the pro-urine via the epithelial Mg^{2+} channel TRPM6 is primarily driven by the negative potential across the luminal membrane. This luminal membrane potential is maintained by an apical K^+ efflux via Kv1.1 energized by the action of the Na^+/K^+-ATPase. At the basolateral membrane, Mg^{2+} extrusion to the blood side occurs via an unknown mechanism. The identified N255D mutation results in a nonfunctional Kv1.1 channel and thereby decreases the driving force for Mg^{2+} influx, thus resulting in renal Mg^{2+} wasting.

mutations in *KCNA1* thus far have been shown to result in episodic ataxia type 1 (EA1). Figure 1, D and E, shows the previously identified mutations in close proximity to the N255D mutation (17–22). EA1 is a dominant human neurological disorder presumably caused by defective Kv1.1 in the cerebellum. Furthermore, abnormal Kv1.1 activity, originating in the distal motor axons, results in muscle hyperactivity, indicative for myokymia (23, 24). In addition to the classical description of this disorder, phenotypic variants include EA1 with partial epilepsy (18, 19), EA1 without myokymia (20), and isolated neuromyotonia (19). We also analyzed the affected members of our Brazilian family for episodic ataxia. On a cerebral MRI of the proband, we obtained evidence of a slight atrophia of the cerebral vermis (data not shown). Furthermore, electromyographs of some affected members showed myokymic discharge, in line with the previously observed mixed phenotype (data not shown). Now, we present hypomagnesemia as a new phenotypic characteristic associated with a mutation in *KCNA1*. Thus, it would be interesting to perform in the near future a large-scale phenotypical characterization of patients with identified mutations in the *KCNA1* gene, including neurological description, serum Mg^{2+} levels, and functional analysis of the corresponding Kv1.1 mutations.

Previously, genetic studies in familial hypomagnesemia revealed several new proteins with a predominant expression in kidney, underlining its involvement in Mg^{2+} homeostasis. Our immunohistochemical data clearly demonstrated the localization of Kv1.1 along the luminal membrane of TRPM6-expressing DCT cells, consistent with a potential link between Kv1.1-mediated K^+ secretion and Mg^{2+} influx via TRPM6. Therefore, we assessed the role of Kv1.1 in controlling Mg^{2+} influx via TRPM6. Electrophysiological analysis of wild-type Kv1.1 and Kv1.1 N255D revealed that the mutation results in a nonfunctional Kv1.1 channel. Kv1.1 channels consist of 4 subunits arranged symmetrically around an aqueous pore, forming a so-called tetrameric structure (25, 26). It has been shown that Kv1.1 channel subunits can assemble with other Kv channel subunits to form heterotetramers (27). Importantly, hypomagnesemia in the Brazilian family is inherited in an autosomal dominant manner, and patients with the N255D mutation are heterozygous. Expression of both alleles likely results in the formation of heterotetrameric channels composed of wild-type and mutated channel subunits, leading to a dominant negative effect by the Kv1.1 N255D subunit, as shown in this study. The mutation replaces a neutral amino acid (asparagine) with one with an acidic side chain (aspartic acid), which may destabilize the secondary or tertiary channel structure and thereby channel formation or trafficking. However, we demonstrated that wild-type Kv1.1 channels, Kv1.1 N255D channels, and the combination thereof are expressed in equal amounts at the plasma membrane.

Considering the striking localization of Kv1.1 in the TRPM6-expressing DCTs, we investigated a potential direct functional effect of Kv1.1 on TRPM6 activity. However, neither wild-type Kv1.1 nor Kv1.1 N255D altered the TRPM6-mediated Na^+ currents, and it is therefore unlikely that Kv1.1 directly regulates the activity of the Mg^{2+}-permeable channel TRPM6. Mg^{2+} is actively reabsorbed in the DCT. Here, Mg^{2+} influx through TRPM6 is driven by a favorable membrane voltage (6, 7). This membrane potential is maintained by a so-far-unidentified apical K^+ efflux pathway, while the K^+ gradient is provided by the basolaterally localized Na^+/K^+-ATPase. Previously, a mutation in the Na^+/K^+-ATPase γ-subunit was shown to be the underlying cause of autosomal dominant renal Mg^{2+} wasting and secondary hypocalciuria (11). Interestingly, K^+ efflux through K^+-permeable channels primarily determines the resting membrane potential. Kv channels are widely expressed in excitable and nonexcitable cells, where they play an essential role in the establishment of the electrical properties of the cell, instrumental for many processes (28). By use of the current clamp mode of the patch clamp technique, we demonstrated that the plasma membrane is hyperpolarized to a significant extent in Kv1.1- compared with mock or Kv1.1 N255D–transfected cells. This effect was reversible by DTX-K, a specific Kv1.1 channel blocker, confirming the involvement of Kv1.1 in setting the negative membrane potential. We now hypothesize that the voltage-gated Kv1.1 channel is responsible for the establishment of the negative membrane potential across the luminal membrane of the DCT cell. The N255D mutation leads to depolarization of the luminal membrane, notably diminishing the driving force for Mg^{2+} uptake from the pro-urine (Figure 4).

In conclusion, our study discloses a new direct coupling between K^+ secretion and active Mg^{2+} reabsorption, which is highlighted by our discovery of the N255D mutation in the *KCNA1* gene in autosomal dominant hypomagnesemia. The encoded K^+ channel Kv1.1 colocalizes with the Mg^{2+} influx channel TRPM6 along the luminal membrane of DCT, the main site of active renal Mg^{2+} reabsorption. Kv1.1 channels harboring the N255D mutation show near-background currents, impairing their ability to set a membrane potential that favors TRPM6-mediated Mg2$^+$ influx. These findings will open a new window for other studies on the interrelationship of renal K^+ and Mg^{2+} disturbances.

Methods

Subjects. The study was approved by the Clinical Hospital, Parana Federal University (Curitiba, Paraná, Brazil), and written informed consent was obtained from the subjects. We identified a large family (46 family mem-

bers, 21 affected) with autosomal dominant hypomagnesemia (Figure 1A). The phenotype in the proband (IV-3) starting from infancy included recurrent muscle cramps, tetanic episodes, tremor, and muscle weakness, especially in distal limbs. There were no seizures, recurrent urinary tract infections, polyuria, polydipsia, or renal stones. At 4 years the patient was determined to have significant hypomagnesemia (0.37 mmol/l; normal, 0.70–0.95 mmol/l). Serum K^+ (3.9 mmol/l; normal, 3.5–5.0 mmol/l), Ca^{2+} (2.35 mmol/l; normal, 2.15–2.50 mmol/l), sodium, phosphate, uric acid, bicarbonate, urea, creatinine, glucose, bilirubin, aminotransferases, alkaline phosphate, and lactate dehydrogenase were all normal. Urinary creatinine clearance, urinary Mg^{2+} excretion (2.8 mmol/24 h; normal 2.1–6.2 mmol/24 h), and Ca^{2+} excretion were also normal. The patient received a daily dose of magnesium chloride, which improved muscular weakness, but slight muscle cramps persisted, particularly after physical activity. One of her younger brothers (IV-1, Figure 1A) died in infancy from a severe attack of cramps and tetany. At that time, the serum Mg^{2+} level was as low as 0.28 mmol/l. In addition, 18 other family members had shown similar clinical manifestations and biochemical features. The proband was tested for signs of cerebellar dysfunction and reported having experienced several periods during which she was not able to walk straight. Objective clinical signs of cerebellar dysfunction, including nystagmus, multistep or overshoot saccades, dysmetria in the finger-nose test, and decomposition of movement of the legs on heel-to-shin test, were absent. However, on a cerebral MRI of the proband, we found evidence of slight atrophia of the cerebral vermis (data not shown). Furthermore, electromyographs of some affected members showed myokymic discharge in line with the previously observed mixed phenotype. We collected blood samples of the family members (both affected and nonaffected; Figure 1A) for linkage analysis. Subsequently, DNA was extracted according to standard protocols. Control genomic DNA samples (n = 100) were provided by H. van Bokhoven (Department of Human Genetics, Radboud University Nijmegen Medical Centre).

Genetic linkage analysis. A genome-wide linkage approach was performed for 12 family members selected based on simulations in SLINK (29) using the Affymetrix GeneChip Mapping 10K 2.0 Array harboring 10,204 SNPs. Sample preparation and hybridization were performed according to the manufacturer's protocol (Affymetrix) (30). Briefly, 250 ng of genomic DNA was digested using 10 U *Xba*I (Westburg), followed by ligation using T4 DNA ligase (Westburg) of universal adaptors to the digested products. Primers complementary to the adaptors were used for amplification of the digested products. After purification of the products using MinElute plates (QIAGEN), fragmentation was performed on 20 μg purified PCR product. Fragmented products were end-labeled and hybridized to the Affymetrix 10K GeneChip overnight. Hybridized arrays were washed and stained using the Fluidics Station 400 (Affymetrix). The GeneChip Scanner 3000 was used to scan the hybridized arrays. Automatic SNP calls were generated using GeneChip DNA analysis software (GDAS; Affymetrix). SNP calls are AA or BB for homozygous SNPs, AB for heterozygous SNPs. When the software was unable to make a call (AA, BB, or AB), the SNP was scored as "no call." Merlin software (www.sph.umich.edu/csg/abecasis/Merlin/index.html) was used to calculate lod scores. Eight microsatellite markers (D12S1626, D12S1725, D12S99, D12S374, D12S1623, D12S336, D12S77, and D12S89) were selected to fine-map the newly identified hypomagnesemia loci on the short arm of chromosome 12 (Human Genome Browser Gateway; http://genome.ucsc.edu/cgi-bin/hgGateway). Marker analysis using fluorescently labeled primers was performed according to the protocol for Linkage Mapping Set MD10 version 2.5 (Applied Biosystems). Reactions for each marker were performed separately, with products being pooled into size- and label-specific sets before typing. Markers were typed on an ABI 3730 DNA analyzer (Applied Biosystems) using GeneMapper 4.0 software (Applied Biosystems). Allele binning was performed with the Excel 2000 (Microsoft) macro linkage designer developed by van Camp and coworkers (31), and we checked Mendelian inheritance of alleles with PedCheck 1.0 software (http://watson.hgen.pitt.edu/register/docs/pedcheck.html) (32). Multipoint lod score and haplotype analysis was performed with GeneHunter, version 2.1 release 5, in the easyLINKAGE software package (33) and Haplopainter software (haplopainter.sourceforge.net/html/index.html).

Mutation analysis. From the critical region, we selected the *KCNA1* gene for mutation analysis, using the UCSC Genome Browser database (http://genome.ucsc.edu/). DNA amplification reactions were performed in a thermal cycler with heated lid (PTC-200; MJ Research). The *KCNA1* exon sequence and flanking regions were amplified from genomic DNA of individual III-1 (Figure 1A) using multiple overlapping primer sets based on GenBank accession code BC101733 (Supplemental Table 1). PCR products of correct sizes were selected by DNA agarose gel electrophoresis, following excision and subsequent purification with GenElute Gel Extraction Kit (Sigma-Aldrich) according to the manufacturer's protocol. The fragments were sequenced on both strands by use of the ABI PRISM Big Dye Terminator v2.0 Ready Reaction Cycle Sequencing Kit and the ABI PRISM 3730 DNA analyzer (Applied Biosystems).

Immunohistochemistry. Immunohistochemistry was performed as previously described (34). In short, either coimmunohistochemical staining or staining of serial sections for Kv1.1 with TRPM6, calbindin D_{28K}, and AQP2 was performed on 7-μm sections of fixed frozen mouse kidney samples. The mouse kidney cryosections were incubated for 16 hours at 4°C with the following primary antibodies: rabbit anti-Kv1.1 (1:300) (APC-009; Alomone Labs), guinea pig anti-TRPM6 (1:1,000) (6), guinea pig anti-AQP2 (1:1,000) (provided by P.M.T. Deen, Department of Physiology, Radboud University Nijmegen Medical Centre), and mouse anti–calbindin D_{28K} (1:750) (35). For detection of calbindin D_{28K} and AQP2, sections were incubated with Alexa Fluor–conjugated secondary antibodies. The Tyramide Signal Amplification kit (PerkinElmer) was used after incubation with biotin-coated goat anti-rabbit and goat anti–guinea pig secondary antibodies to visualize Kv1.1 and TRPM6, respectively. Images were taken with a confocal laser scanning imaging system (FluoView FV1000; Olympus).

DNA constructs. The *KCNA1* wild-type and N255D mutant sequences were obtained by amplification of genomic DNA from a nonaffected and affected family member, respectively, using primers 5′-GCCGAATTCGGCCACCATGACGGTGATGTC-3′ and 5′-GCCGTCGACATGCAACAACGCATTGACAG-3′. Both PCR products were cloned into pCMV-SPORT6 vectors (Invitrogen) using restriction enzymes *Eco*RI and *Sal*I following verification by sequence analysis. Subsequently, both the *KCNA1* wild-type and N255D sequences were subcloned via the Gateway pDONR221 entry vector into a pCIneo IRES-GFP destination clone, creating human *KCNA1* pCIneo IRES GFP (wild-type Kv1.1) and human *KCNA1* N255D pCIneo IRES GFP (Kv1.1 N255D). The pCIneo IRES GFP construct was used as a control (mock) in the experiments. The wild-type TRPM6 pCIneo IRES GFP construct has been described previously (6).

Electrophysiology. HEK293 cells were cultured and transfected as described previously (36). Whole-cell recordings were performed as described in a previous study (14). Recorded Kv1.1 currents were evoked as described previously, using the same standard pipette and bath solutions (37). The membrane potential of transfected HEK293 cells was measured using the current clamp mode, with continuous recording from a holding current of 0 pA. The pipette solution contained (in mM): 140 KCl, 1 Na_2-ATP, 10 HEPES/KOH (pH 7.3). The bath solution contained (in mmol/l): 138 NaCl, 5.4 KCl, 1.2 $MgCl_2$, 1 $CaCl_2$, 10 glucose, and 10 HEPES/KOH (pH 7.3). For measurement of TRPM6-mediated currents, a linear voltage ramp from –100 to +100 mV (within 450 ms) was applied every 2 seconds

from a holding potential of 0 mV. The standard pipette solution contained (in mmol/l): 150 NaCl, 10 EDTA, and 10 HEPES/KOH (pH 7.2). The extracellular solutions contained 150 mmol/l NaCl, 10 mmol/l HEPES/KOH (pH 7.4). The analysis and display of patch clamp data were performed using IGOR Pro software (WaveMetrics). Current densities were obtained by normalizing the current amplitude to the cell membrane capacitance.

Cell surface biotinylation. HEK293 cells were transiently transfected using Lipofectamine 2000 (Invitrogen) with 1 μg DNA of wild-type Kv1.1, 1 μg Kv1.1 N255D, or 1 μg mock plasmid or cotransfected with 0.5 μg wild-type Kv1.1 and 0.5 μg Kv1.1 N255D. Cell surface labeling with biotin was performed as described previously (38). At 48 hours after transfection, the biotinylation assay was performed. Cells were homogenized in 1 ml lysis buffer as described previously (38), using the Sulfo-NHS-LC-LC-Biotin (Pierce; Thermo Scientific). One percent of the total protein amount was collected as an input sample. Subsequently, biotinylated proteins (plasma membrane fraction) were precipitated using NeutrAvidin-agarose beads (Pierce; Thermo Scientific). Kv1.1 expression was analyzed by immunoblot analysis for the input and the plasma membrane fraction using the monoclonal Kv1.1 antibody (1:1,000).

Chemicals. The guinea pig antibody against AQP2 was provided by P.M. Deen (Radboud University Nijmegen Medical Centre). Mouse anti–calbindin D_{28K} was purchased from Sigma-Aldrich. Rabbit polyclonal and mouse monoclonal antibodies specific for Kv1.1 were purchased from Alomone Labs and NeuroMab, for immunohistochemistry and Western blotting, respectively. DTX-K was purchased from Sigma-Aldrich.

Statistics. Data are shown as mean ± SEM. Statistical significance was determined using ANOVA with Tukey's procedure. Differences in means with $P < 0.05$ were regarded as statistically significant. Statistical analysis was performed using Prism (GraphPad) software.

Acknowledgments

The authors are grateful to our colleagues K. Lee, F. van Zeeland, A. Forst, M. Schijvenaars, and R. Makkinje for technical assistance and helpful suggestions and to C. E. Silvado and L.C. Werneck for recruitment of the patients and their relatives. This study was supported financially by the Netherlands Organization for Scientific Research (ZonMw 9120.6110; ALW 700.55.302), a European Young Investigator award from the European Science Foundation, and the Dutch Kidney foundation (C03.6017).

Received for publication July 28, 2008, and accepted in revised form January 7, 2009.

Address correspondence to: René J. Bindels, 286 Physiology, PO Box 9101, 6500 HB Nijmegen, The Netherlands. Phone: 31-24-3614211; Fax: 31-24-3616413; E-mail: r.bindels@ncmls.ru.nl.

1. Wong, E.T., Rude, R.K., Singer, F.R., and Shaw, S.T., Jr. 1983. A high prevalence of hypomagnesemia and hypermagnesemia in hospitalized patients. *Am. J. Clin. Pathol.* **79**:348–352.
2. Chernow, B. 1989. Hypomagnesemia in intensive care. Correction of units. *Chest.* **95**:1362.
3. Konrad, M., Schlingmann, K.P., and Gudermann, T. 2004. Insights into the molecular nature of magnesium homeostasis. *Am. J. Physiol. Renal Physiol.* **286**:F599–F605.
4. Quamme, G.A. 1997. Renal magnesium handling: new insights in understanding old problems. *Kidney Int.* **52**:1180–1195.
5. Dai, L.J., et al. 2001. Magnesium transport in the renal distal convoluted tubule. *Physiol. Rev.* **81**:51–84.
6. Voets, T., et al. 2004. TRPM6 forms the Mg^{2+} influx channel involved in intestinal and renal Mg^{2+} absorption. *J. Biol. Chem.* **279**:19–25.
7. Schweigel, M., Lang, I., and Martens, H. 1999. Mg^{2+} transport in sheep rumen epithelium: evidence for an electrodiffusive uptake mechanism. *Am. J. Physiol.* **277**:G976–G982.
8. Weber, S., et al. 2000. Familial hypomagnesaemia with hypercalciuria and nephrocalcinosis maps to chromosome 3q27 and is associated with mutations in the PCLN-1 gene. *Eur. J. Hum. Genet.* **8**:414–422.
9. Simon, D.B., et al. 1999. Paracellin-1, a renal tight junction protein required for paracellular Mg2+ resorption. *Science.* **285**:103–106.
10. Simon, D.B., et al. 1996. Gitelman's variant of Bartter's syndrome, inherited hypokalaemic alkalosis, is caused by mutations in the thiazide-sensitive Na-Cl cotransporter. *Nat. Genet.* **12**:24–30.
11. Meij, I.C., et al. 2000. Dominant isolated renal magnesium loss is caused by misrouting of the Na^+,K^+-ATPase gamma-subunit. *Nat. Genet.* **26**:265–266.
12. Schlingmann, K.P., et al. 2002. Hypomagnesemia with secondary hypocalcemia is caused by mutations in TRPM6, a new member of the TRPM gene family. *Nat. Genet.* **31**:166–170.
13. Walder, R.Y., et al. 2002. Mutation of TRPM6 causes familial hypomagnesemia with secondary hypocalcemia. *Nat. Genet.* **31**:171–174.
14. Groenestege, W.M., et al. 2007. Impaired basolateral sorting of pro-EGF causes isolated recessive renal hypomagnesemia. *J. Clin. Invest.* **117**:2260–2267.
15. Aggarwal, S.K., and MacKinnon, R. 1996. Contribution of the S4 segment to gating charge in the Shaker K^+ channel. *Neuron.* **16**:1169–1177.
16. Hoenderop, J.G., et al. 2000. Localization of the epithelial Ca^{2+} channel in rabbit kidney and intestine. *J. Am. Soc. Nephrol.* **11**:1171–1178.
17. Browne, D.L., et al. 1994. Episodic ataxia/myokymia syndrome is associated with point mutations in the human potassium channel gene, KCNA1. *Nat. Genet.* **8**:136–140.
18. Zuberi, S.M., et al. 1999. A novel mutation in the human voltage-gated potassium channel gene (Kv1.1) associates with episodic ataxia type 1 and sometimes with partial epilepsy. *Brain.* **122**:817–825.
19. Eunson, L.H., et al. 2000. Clinical, genetic, and expression studies of mutations in the potassium channel gene KCNA1 reveal new phenotypic variability. *Ann. Neurol.* **48**:647–656.
20. Lee, H., et al. 2004. A novel mutation in KCNA1 causes episodic ataxia without myokymia. *Hum. Mutat.* **24**:536.
21. Klein, A., Boltshauser, E., Jen, J., and Baloh, R.W. 2004. Episodic ataxia type 1 with distal weakness: a novel manifestation of a potassium channelopathy. *Neuropediatrics.* **35**:147–149.
22. Shook, S.J., Mamsa, H., Jen, J.C., Baloh, R.W., and Zhou, L. 2008. Novel mutation in KCNA1 causes episodic ataxia with paroxysmal dyspnea. *Muscle Nerve.* **37**:399–402.
23. da Silva, A.B., Japp, H.H., Saldanha, A., and Henriques, F.G. 1977. Isaacs' syndrome. Report of a case and review of the literature [In Portuguese]. *Arq. Neuropsiquiatr.* **35**:139–145.
24. Newsom-Davis, J., and Mills, K.R. 1993. Immunological associations of acquired neuromyotonia (Isaacs' syndrome). Report of five cases and literature review. *Brain.* **116**:453–469.
25. Li, M., Jan, Y.N., and Jan, L.Y. 1992. Specification of subunit assembly by the hydrophilic amino-terminal domain of the Shaker potassium channel. *Science.* **257**:1225–1230.
26. Baumann, A., Grupe, A., Ackermann, A., and Pongs, O. 1988. Structure of the voltage-dependent potassium channel is highly conserved from Drosophila to vertebrate central nervous systems. *EMBO J.* **7**:2457–2463.
27. Shamotienko, O.G., Parcej, D.N., and Dolly, J.O. 1997. Subunit combinations defined for K^+ channel Kv1 subtypes in synaptic membranes from bovine brain. *Biochemistry.* **36**:8195–8201.
28. Armstrong, C.M., and Hille, B. 1998. Voltage-gated ion channels and electrical excitability. *Neuron.* **20**:371–380.
29. Ott, J. 1989. Computer-simulation methods in human linkage analysis. *Proc. Natl. Acad. Sci. U. S. A.* **86**:4175–4178.
30. Matsuzaki, H., et al. 2004. Genotyping over 100,000 SNPs on a pair of oligonucleotide arrays. *Nat. Methods.* **1**:109–111.
31. Van Camp, G., et al. 1997. Linkage analysis of progressive hearing loss in five extended families maps the DFNA2 gene to a 1.25-Mb region on chromosome 1p. *Genomics.* **41**:70–74.
32. O'Connell, J.R., and Weeks, D.E. 1998. PedCheck: a program for identification of genotype incompatibilities in linkage analysis. *Am. J. Hum. Genet.* **63**:259–266.
33. Collin, R.W., et al. 2007. Involvement of DFNB59 mutations in autosomal recessive nonsyndromic hearing impairment. *Hum. Mutat.* **28**:718–723.
34. Hoenderop, J.G., et al. 2002. Modulation of renal Ca^{2+} transport protein genes by dietary Ca^{2+} and 1,25-dihydroxyvitamin D_3 in 25-hydroxyvitamin D_3-1alpha-hydroxylase knockout mice. *FASEB J.* **16**:1398–1406.
35. Bindels, R.J., Hartog, A., Timmermans, J.A., and van Os, C.H. 1991. Immunocytochemical localization of calbindin-D28k, calbindin-D9k and parvalbumin in rat kidney. *Contrib. Nephrol.* **91**:7–13.
36. Chang, Q., et al. 2005. The beta-glucuronidase klotho hydrolyzes and activates the TRPV5 channel. *Science.* **310**:490–493.
37. Jiang, B., Sun, X., Cao, K., and Wang, R. 2002. Endogenous Kv channels in human embryonic kidney (HEK-293) cells. *Mol. Cell. Biochem.* **238**:69–79.
38. Gkika, D., et al. 2006. Tissue kallikrein stimulates Ca^{2+} reabsorption via PKC-dependent plasma membrane accumulation of TRPV5. *EMBO J.* **25**:4707–4716.